Reversible devitrification in amorphous As_2Se_3 under pressure

Azkar Saeed Ahmad,[1] Hong-Bo Lou,[1] Chuan-Long Lin,[1] Ai-Guo Li,[2] Ke Yang,[2] K. Glazyrin,[3] H. P. Liermann,[3] Hermann Franz,[3] Kenny Ståhl,[4] Shuo Cui,[5] Bruno Bureau,[5] Dong-Xian Zhang,[6] Xiao-Dong Wang,[1] Qing-Ping Cao,[1] A. Lindsay Greer,[7] and Jian-Zhong Jiang[1,*]

[1]*International Center for New-Structured Materials and Laboratory of New-Structured Materials, State Key Laboratory of Silicon Materials, School of Materials Science and Engineering, Zhejiang University, Hangzhou 310027, People's Republic of China*

[2]*Shanghai Institute of Applied Physics, Chinese Academy of Sciences, Shanghai 201203, People's Republic of China*

[3]*Photon Science, Deutsches Elektronen-Synchrotron (DESY), Notkestraße 85, D-22603 Hamburg, Germany*

[4]*Department of Chemistry, Building 207, Technical University of Denmark, DK-2800 Lyngby, Denmark*

[5]*Sciences Chimiques de Rennes-EquipeVerres et Céramiques, Université de Rennes 1, France*

[6]*State Key Laboratory of Modern Optical Instrumentation, Zhejiang University, Hangzhou 310027, People's Republic of China*

[7]*Department of Materials Science & Metallurgy, 27 Charles Babbage Road, University of Cambridge, Cambridge CB3 0FS, United Kingdom*

(Received 20 April 2016; published 28 November 2016)

In pressure-induced reversible structural transitions, the term "reversible" refers to the recovery of the virgin structure in a material upon complete decompression. Pressure-induced amorphous-to-crystalline transitions have been claimed to be reversible, but evidence that amorphous material recovers its virgin amorphous structure upon complete depressurization has been lacking. In amorphous As_2Se_3 (a-As_2Se_3) chalcogenide, however, we report a novel reversible amorphous-to-crystalline transition that provides compelling experimental evidence that upon complete decompression, the recovered amorphous phase is structurally the same as that of the virgin (as-cast) amorphous phase. Combining the experimental results with *ab initio* molecular dynamics simulations, we elucidate that the amorphization is mediated by a surplus of total free energy in the high-pressure face-centered cubic phase as compared to the virgin amorphous phase and that the structural recovery to the virgin amorphous phase is a consequence of an enhancement in covalent bonding character over interlayer forces upon complete decompression. Furthermore, we observed a two-dimensional to three-dimensional network transition under compression and its reversibility upon decompression.

DOI: 10.1103/PhysRevB.94.195211

I. INTRODUCTION

Ever since it was claimed [1] that crystalline $AlPO_4$ exhibits a "reversible" crystalline-to-amorphous transition under pressure, efforts have been dedicated [2–7] to the challenge of studying pressure-induced reversible crystalline-to-amorphous transitions. However, for amorphous materials, little attention has been paid to elucidating and verifying the converse phenomenon of reversible amorphous-to-crystalline transitions under pressure. Most likely, the problem that hinders scientists in verifying the reversible amorphous-to-crystalline transition is lack of knowledge concerning the exact atomic packing in amorphous materials before compression and after the compression-decompression cycle. To our knowledge, Kalkan *et al.* [8] have made the only attempt to hunt for structural reversibility by comparing the structure of as-prepared amorphous GaSb (a-GaSb) and the amorphous obtained after the specimen was fully released from the high-pressure crystalline phase. However, a-GaSb was unable to recover its virgin amorphous phase and was transformed to a new amorphous phase (high-density amorphous phase) upon complete decompression. Furthermore, pressure-induced amorphous-to-crystalline transitions in a-Si [9], a-$Ge_2Sb_2Te_5$ [10], and decompressed-amorphized GaSb and (GaSb)-Ge_2 [11–16] had also been claimed to be reversible. But in these papers, comparison between the as-prepared amorphous and the amorphous recovered from the high-pressure crystalline phase has not been made. Keeping in mind the example of a-GaSb [8] (which was transformed to a new amorphous phase upon decompression) and the possibility of the occurrence of an amorphous-to-amorphous phase transition under decompression [17,18], the recovered amorphous could be structurally different from the as-prepared amorphous. In this regard, without experimental evidence (i.e., without structural comparison between the recovered amorphous and the as-prepared amorphous), the claim for the reversible amorphous-to-crystalline transition remains ambiguous and questionable. One can only claim for the reversible amorphous-to-crystalline transitions, provided the recovered amorphous has essentially the same phase (same structure) as that of the virgin amorphous phase. Here, in a-As_2Se_3 chalcogenide, employing four pressure media in synchrotron-radiation x-ray diffraction (XRD) and Raman spectroscopy measurements, we provide first unambiguous experimental evidence for the novel pressure-induced reversible amorphous-to-crystalline transition in which the virgin amorphous phase is recovered upon complete decompression.

II. MATERIALS AND METHODS

A. Sample preparation

The residual oxygen content in arsenic and selenium samples of 99.999% purity was reduced using the volatilization technique. The vapor pressure of the oxides of these metals is greater than that of the metals themselves; this is exploited

*Corresponding author: jiangjz@zju.edu.cn

to remove the oxide species. Selenium was heated at 250 °C and arsenic was heated at 290 °C under vacuum for several hours. After this treatment, the required amounts of As and Se were sealed in a silica tube under vacuum. This mixture was maintained at 650 °C for 12 h in a rocking furnace to ensure good mixing and homogenization of the liquid. To condense a maximum of vapor into the liquid, the temperature was reduced to 500 °C for 1 h. Then the ampoules were quenched in air and later annealed near the glass-transition temperature of As_2Se_3 ($T_g \approx 200$ °C) for 10 h to reduce the mechanical stresses induced during cooling. The amorphous nature of the As_2Se_3 sample was confirmed by XRD and differential scanning calorimetry.

B. *In situ* measurements at high pressure

Raman and synchrotron radiation XRD experiments were performed in a Mao-Bell-type diamond anvil cell (DAC) with a culet 300 μm in diameter. The sample chamber was a hole of ~100 μm diameter drilled in a preindented T301 stainless steel gasket. The specimen was loaded into the sample chamber, along with ruby as a pressure standard for calibration. To verify that the pressure-induced transitions are a function of hydrostatic pressure alone, four pressure media (Ne, Ar, silicon oil, and a 4:1 mixture of methanol to ethanol) were used in more than 10 experimental runs reaching similar pressure ranges.

Angle-dispersive XRD measurements were performed *in situ* under high pressure at the beamline P02.2, PETRAIII, Deutsches Elektronen-Synchrotron (DESY), Hamburg, Germany, and at the beamline BL15U, Shanghai Synchrotron Radiation Facility (SSRF), Shanghai, P.R. China. For the data presented here, the energy of the synchrotron radiation was adjusted to 42.7 keV. Two-dimensional (2D) diffraction patterns were collected using a PerkinElmer 1621 ScI-bonded amorphous silicon 2D detector (2048×2048 pixels, 200×200-μm pixel size) mounted orthogonal to the direction of the incident x-ray beam. A CeO_2 standard was used to measure the sample-to-detector distance and the tilt of the detector relative to the beam path. The sample was exposed to an x-ray beam with a cross-section of 8×3 μm^2 for 5 min. For each pressure step, 30 scans were made on the sample, followed by the same number of background correction scans, which were later used for background subtraction. These background correction scans were collected on the pressure medium, away from the sample and pressure markers (ruby chips). The 2D patterns were integrated into Q space using the software package Fit2D [19].

Raman experiments were performed using a Renishaw microscope at the International Centre of New-Structured Materials, Zhejiang University, P.R. China, using a laser of wavelength of 785 nm. The laser power was set to 5 mW after optimization to avoid heat- and photo-induced degradation while still enabling the collection of high-quality Raman spectra.

C. Molecular dynamics simulations

Ab initio molecular dynamics (AIMD) simulations were performed using the Vienna *Ab initio* Simulation Package (VASP) code [20] and the projector-augmented wave (PAW) method [21,22] with generalized gradient approximations. A supercell containing 180 atoms (72 As and 108 Se) was quenched from 2000 K to room temperature (RT) at 0.33 K/fs, and the Nose thermostat [23] was used to control the temperature. The mass density was fixed at the measured value for a-As_2Se_3 (~4.31 g/cm^3) [24], and the zero-pressure density was obtained by relaxing the box. After quenching to RT, the system was equilibrated for 4000 time steps (3 fs/step), and pressure was applied by uniformly reducing the volume of the box. This method of application of pressure mimics experimental hydrostatic compression and has been previously adopted in many AIMD studies on pressure-induced structural changes. When comparing simulations with experimental results, the spatiotemporal limitation of the AIMD simulations must be taken into account. In the present paper, the small size of the box (180 atoms) may cause statistical fluctuations and lead to different structures. However, the general trend in structural evolution can still be identified.

III. RESULTS AND DISCUSSION

Figures 1(a) and 1(b) shows XRD patterns of a-As_2Se_3 in Q space during compression and decompression, respectively. Under ambient conditions, and persisting to some extent as the pressure is increased, there is a prepeak in the XRD patterns near $Q = 1.3$ Å^{-1}; this corresponds to a 2D layered structure [25–29]. As the pressure is increased, the prepeak shifts to higher Q values and loses intensity, finally disappearing ~13.5 GPa [Fig. 1(a)]. The loss of this peak reflects the destruction of the intermediate range order (IRO) associated with the layered structure and marks the completion of the transition from a two-dimensional (2D) to a three-dimensional (3D) amorphous network. The progress of this transition and the pressures over which it occurs are consistent with the infrared (IR) spectroscopy measurements of Struzhkin *et al.* [30]. At ~40.5 GPa, the specimen crystallizes into a face-centered cubic (fcc) structure with a cell parameter of ~9.8 Å, and this crystalline phase remains stable up to 53.5 GPa, the highest pressure achieved during the synchrotron-radiation XRD measurements. Upon decompression, the high-pressure crystalline phase remains stable down to ~34.3 GPa, below which this phase reverts gradually to the amorphous phase. The transition back to the amorphous phase is completed, within experimental uncertainty, when the pressure reaches 0.1 GPa [Fig. 1(b)].

Figures 2(a) and 2(b) shows the high-pressure behavior of a-As_2Se_3 observed with Raman spectroscopy. At ambient pressure, the Raman spectrum of a-As_2Se_3 consists of a main asymmetric envelope ~225 cm^{-1}, corresponding to the interlayer vibrations of pyramidal $AsSe_3$ units (which are the basic building blocks of the layered structure in a-As_2Se_3), and a faint broad peak ~460 cm^{-1}, corresponding to As-Se vibrations [31]. When the pressure is increased, the intensity of the main envelope decreases and it shifts to higher frequencies. Finally, the main envelope vanishes ~14 GPa, suggesting completion of the 2D-to-3D network transition. As the layers are forced closer, the $AsSe_3$ pyramidal units are distorted (i.e., the As-Se-As bond angle is changed). As a result, the band representing the vibrations of $AsSe_3$ pyramidal units is broadened and reduced in intensity. This behavior is in good agreement with the XRD results in Fig. 1(a) and explains the

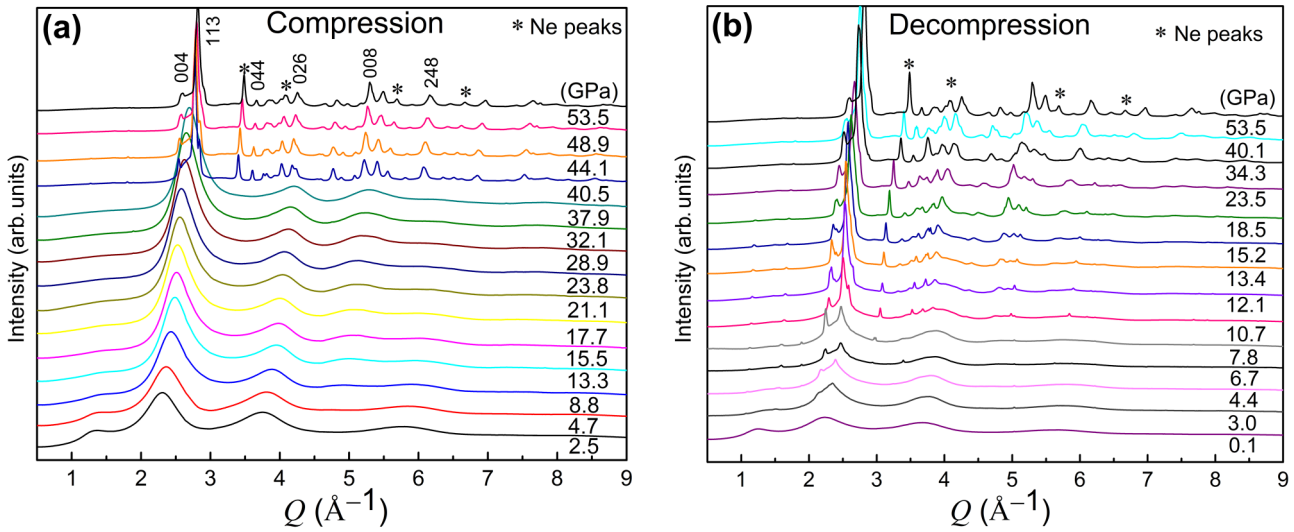

FIG. 1. *In situ* high-pressure XRD patterns of a-As_2Se_3 at RT in a DAC. (a) Integrated XRD patterns at selected pressures during compression up to 53.5 GPa; the main diffraction peaks of the fcc phase are indexed. (b) Integrated XRD patterns at selected pressures during decompression from 53.5 to 0.1 GPa. Ne was used as pressure-transmitting medium for the results shown in (a) and (b). We observed a similar reversible amorphous-to-crystalline transition when the synchrotron-radiation XRD measurements were performed with other pressure-transmitting media (see Supplemental Material [32], particularly Fig. S3).

kink observed in the band gap measurements [30]. With a further increase in pressure, ∼36 GPa, two new peaks appear ∼325 and ∼600 cm^{-1}, indicating the onset of crystallization. This crystalline phase remains stable up to 51.3 GPa, which was the highest pressure achieved in the Raman-scattering measurements. During decompression, the crystalline peaks start to disappear ∼37 GPa. With a further decrease in pressure, ∼11 GPa, the peak indicative of the amorphous phase starts to reappear, and it is fully recovered when the pressure is completely released. In the Raman-scattering measurements, the onset of the crystallization during compression and the onset of the vitrification during decompression are earlier than in the XRD measurements. The apparent hysteresis is very low, because the Raman scattering is highly sensitive to the local structure.

As noted earlier, the nature of the amorphous phase recovered on decompression may be of particular interest for potential device applications. In the present work, the initial amorphous phase, obtained by bulk casting of the liquid, is likely to be relaxed in comparison with the deposited thin films commonly used in other studies. This initial phase therefore provides a good basis for assessment of the structural

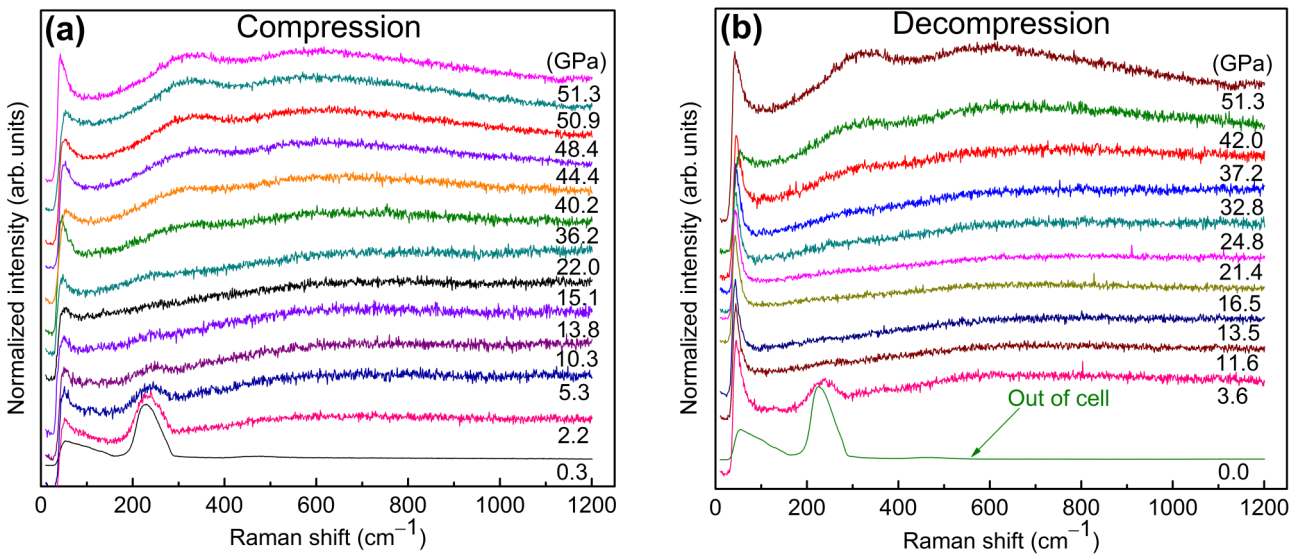

FIG. 2. *In situ* high-pressure Raman spectroscopy results for a-As_2Se_3 at RT. (a) Raman spectra at selected pressures during compression up to 51.3 GPa. (b) Raman spectra at selected pressures during decompression from 51.3 to 0 GPa. Ar was used as pressure-transmitting medium for the results shown in (a) and (b). We observed a similar reversible amorphous-to-crystalline transition when the Raman-scattering measurements were performed with other pressure-transmitting media (see Supplemental Material [32], particularly Figs. S4 and S5).

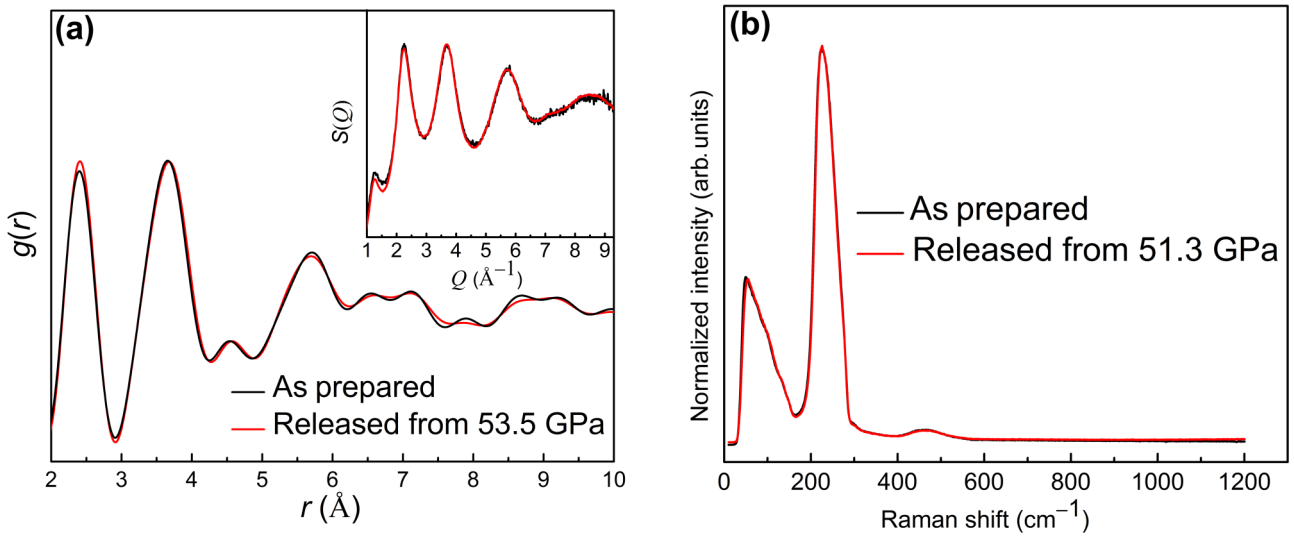

FIG. 3. Comparison of XRD and Raman spectra of an as-cast a-As_2Se_3 sample and a sample recovered from the high-pressure fcc crystal phase. (a) The total pair-distribution function $g(r)$ and structure factor $S(Q)$ (inset) for the as-cast sample and for a sample fully released from 53.5 GPa. (b) Raman spectra of the as-cast sample and a sample fully released from 51.3 GPa. The pressure-induced transitions are fully reversible on decompression, and the recovered amorphous state is essentially identical to the relaxed as-cast state before compression. Ne was used as pressure-transmitting media for the results shown in (a), and Ar was used as pressure-transmitting media for the results shown in (b). Our experimental results with other pressure-transmitting media (see Supplemental Material [32], particularly Fig. S6) confirm the recovery of local structure upon decompression. For amorphous materials, this is the first example of the local structure memory effect in the reversible amorphous-to-crystalline transition.

changes that may be induced by crystallization and reversion to the amorphous phase. For a-As_2Se_3, we compare the pair-distribution functions $g(r)$, structure factors $S(Q)$, and Raman spectra for the as-cast sample (before compression) and the sample after compression and decompression [Figs. 3(a) and 3(b)]. Surprisingly, we observe, within experimental uncertainty, no differences between the two samples in terms of positions and intensities in $g(r)$, $S(Q)$, or the Raman spectra [Figs. 3(a) and 3(b)] (see Supplemental Material [32], particularly Figs. S6(a) and S6(b)). These results suggest that the RT pressure-induced crystallization in a-As_2Se_3, when reversed, gives an amorphous phase that is remarkably relaxed and similar to the bulk as-cast state. Such a high degree of reversibility is unusual in studies on other chalcogenides, and is the first example of local structure memory in reversible amorphous-to-crystalline transitions in amorphous materials.

We explore the origin of this reversibility by performing AIMD simulations on the effects of pressure on a-As_2Se_3. Despite the difference of predicted and observed transition pressure values (Fig. 4), our simulations correspond well with the experimental findings on the nature of the phase changes. Specifically, the amorphous-to-crystalline phase transition during compression and the crystalline-to-amorphous phase transition during decompression were well reproduced by the simulations (Fig. 4). Upon compression, the first peak of $g(r)$ moves to higher r values and the second peak starts to merge into the first peak. Again, in good agreement with our experiments, this behavior is an indication of change in the covalent bonding character at the onset of the 2D-to-3D network transition. After the completion of this transition, with further increase in pressure, the second peak is completely merged into the first peak, and the first peak starts to move to shorter r, accompanying densification. At a pressure of 107.8 GPa, we observe the onset of crystallization, as evident from the $g(r)$ curve in Fig. 4(a). This crystalline phase remains stable up to 196.9 GPa, which was the highest pressure achieved in AIMD simulation studies. During decompression, the crystalline phase remains relatively stable down to 39.3 GPa [Fig. 4(b)]. Below this pressure, the specimen enters the amorphous state; the second peak in $g(r)$ starts to reappear and becomes pronounced at 16.1 GPa. The large hysteresis reported in the AIMD studies can be expected, because the small sample size and rapid pressure changes hinder nucleation of phase changes.

This recovery of the second peak in $g(r)$ during decompression indicates that the character of the bonding is increasingly covalent, associated with a reversion to the original 2D amorphous network. From AIMD simulations, the overall $g(r)$ of the sample released from 196.9 GPa is found to match well with the $g(r)$ of the starting sample (before compression), as evident from Fig. 4(c), and this is consistent with the experimental results (Fig. 3). Within the uncertainty, average bond lengths (Supplemental Material, Table SI [32]) and average coordination numbers (CNs) (Supplemental Material, Table SII [32]) are found to be the same for both the as-prepared amorphous and the amorphous obtained after the complete decompression from 196.9 GPa. These results demonstrate the local structure memory in a-As_2Se_3 under pressure (for a detailed discussion, see Supplemental Material [32]). The total free energy of the specimen as a function of pressure [Fig. 4(d)] clearly shows the amorphous-to-crystalline phase transition (during compression) and the reverse transition (during decompression). During compression, the free energy of the amorphous specimen increases linearly (red line) to 107.8 GPa (the onset pressure for crystallization). Above this pressure, the free energy of the crystalline specimen increases

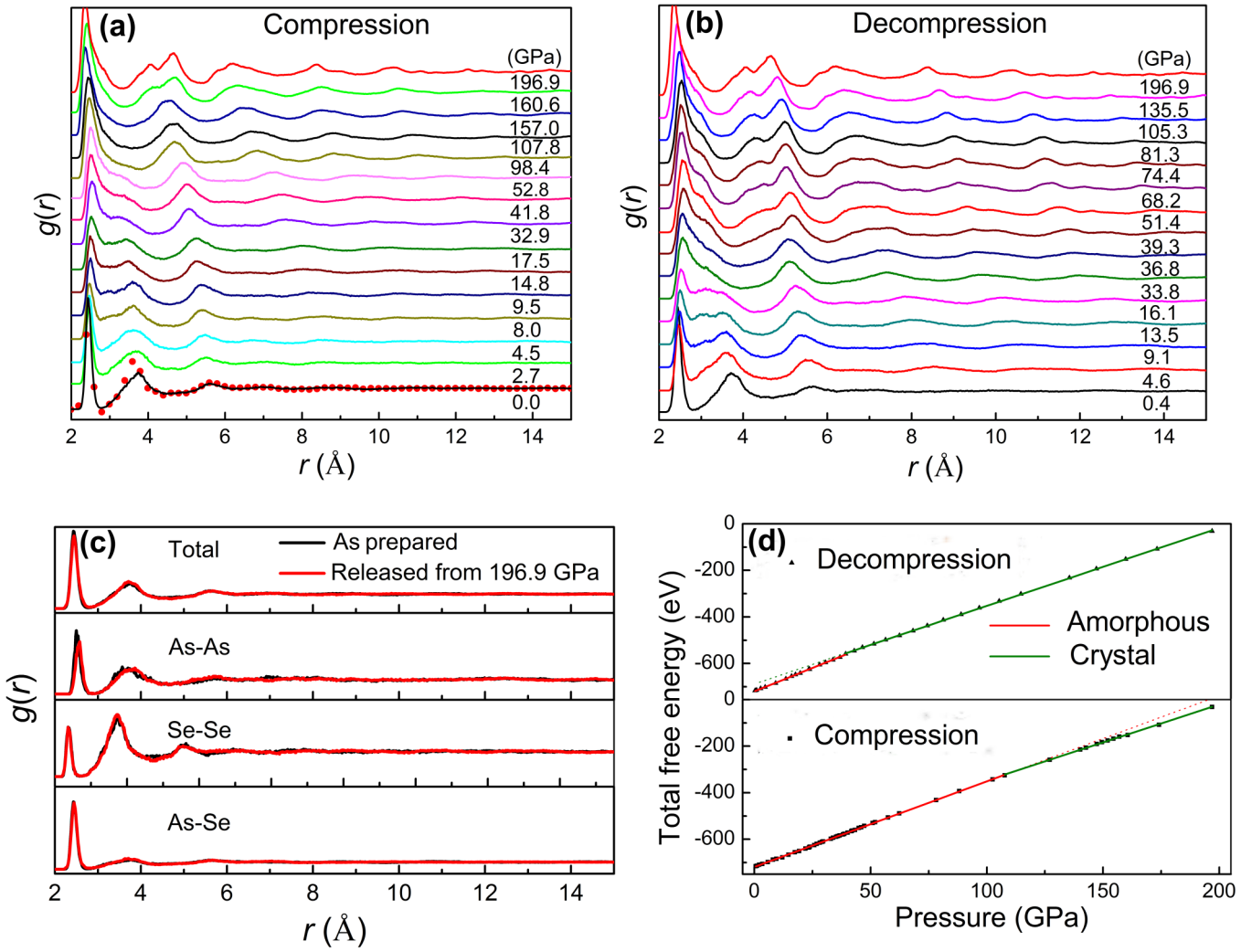

FIG. 4. High-pressure AIMD simulations of a-As_2Se_3 up to 196.9 GPa. (a) Total pair-distribution functions $g(r)$ at selected pressures from simulations (solid lines), together with experimental results (red circles). (b) Total pair-distribution functions $g(r)$ at selected pressures from simulations during decompression. (c) Comparison of total and partial As-As, Se-Se, and As-Se pair-distribution functions, showing that these are similar for the as-prepared amorphous (black line) and the amorphous obtained after complete decompression from 196.9 GPa (red line). (d) Total free energy of the specimen on compression and decompression. The red lines represent the amorphous phase, and the green lines represent the crystalline phase obtained during compression.

linearly (green line), with a lower slope, to the maximum pressure (i.e., 196.9 GPa). The reduced slope of the green line indicates that the specific volume of the crystalline phase is lower than that of the amorphous phase. During decompression, the free energy of the crystalline specimen decreases linearly to 39.3 GPa (green line). Thereafter, the free energy of the amorphous phase again shows a linear, but stronger, pressure dependence (red line) until the complete release of pressure. The free energy of the sample compressed to 196.9 GPa and brought back to ambient conditions is less than 0.05% different from that of the as-cast amorphous sample. It can be concluded that the pressure-induced amorphous-to-crystalline phase transition in a-As_2Se_3 is fully reversible in terms of both thermodynamics and structure.

High-pressure studies on a-As_2S_3 (isostructural with a-As_2Se_3) have revealed that a gradual increase in pressure results in elongation of the As-S bonds because of an increase in the CN [33]. A similar trend is observed for a-As_2Se_3: the first peak in $g(r)$ moves to higher r, the increased average bond length again being attributable to an increased CN, and this scenario is consistent with the recent experimental studies on a-As_2Se_3 [34]. In the case of a-As_2S_3, increasing pressure induces metallic bonding, and we speculate that a similar increase in the metallic character of the bonding in the 3D network a-As_2Se_3 may occur above 30 GPa [30,35]. Our analysis of optical reflectivity (see Supplemental Material [32], particularly Fig. S2) gives an indication of increased metallic character in 3D a-As_2Se_3 before crystallization. While increasing pressure initially results in the 2D-to-3D network transition [evident from the Fig. 4(a)] associated with enhancement of interlayer forces, it subsequently induces a denser metallic state similar to that in isostructural a-As_2S_3 [33]. A further increase in pressure results in crystallization, which with some hysteresis, is reversible upon decompression.

From Fig. 4(b), it is evident that on decompression, vitrification takes place gradually and the second peak in $g(r)$ starts to recover, an indication of the enhancement in covalent bonding. Upon complete decompression, the specimen recovers itself to a covalently bonded 2D-network structure, and within the experimental uncertainty is the same as the as-cast sample [Figs. 3(a) and 3(b) and 4(c) and 4(d) and Tables SI and SII] (see Supplemental Material [32], particularly Figs. S6(a) and S6(b)). The total free energy is the parameter that determines the thermodynamic stabilities of the phases. We calculated the free energies of a-As_2Se_3 and two crystalline phases of As_2Se_3, i.e., the equilibrium monoclinic phase and the high-pressure fcc phase. The order of stability is as follows: monoclinic $>$ amorphous $>$ fcc. On decompression, the fcc phase reverts to the metastable parent 2D-network amorphous phase, rather than to the stable monoclinic phase.

In summary, we have used *in situ* high-pressure synchrotron radiation XRD and Raman scattering to characterize the changes in a-As_2Se_3 on compression to $>$50 GPa and on subsequent decompression. These changes have also been studied in AIMD simulations. We found a reversible change in the amorphous phase from a covalent 2D network to, at higher pressure, a 3D network $\sim$14 GPa and a reversible pressure-induced crystallization to an fcc phase $\sim$36 GPa, with a large kinetic hysteresis. On decompression, after reversal of the crystallization and of the 2D-to-3D transition, the re-formed amorphous phase is in a well-relaxed state essentially indistinguishable from the original bulk as-cast glass. We speculate that this ability to return to a well-defined amorphous state is facilitated by its having a covalent network that is 2D rather than 3D in character. Such structural reversibility and reproducibility in pressure-driven transitions will be useful in identifying systems of interest for phase-change memory. This work clearly provides solid evidence for the existence of a local structure memory effect in reversible crystallization reaction, which may occur in other glassy or amorphous systems, opening a new area of research on studying reversible crystallization reactions.

ACKNOWLEDGMENTS

The authors thank E. Ma and H.-K. Mao for useful discussions. Financial support from the National Basic Research Program of China (Grant No. 2012CB825700), National Natural Science Foundation of China (Grants No. 51371157 and No. U1432105), and Fundamental Research Funds for the Central Universities are gratefully acknowledged. The computer resources at the National Supercomputer Center in Tianjin and Guangzhou and the calculations performed on TianHe-1 (A) are gratefully acknowledged. Synchrotron radiation experiments were carried out at the SSRF, Shanghai, China, and the light source PETRAIII at DESY, a member of the Helmholtz Association (HGF). A.L.G. acknowledges support from the Engineering and Physical Sciences Research Council (UK).

A.S.A. and H.-B.L. contributed equally to this work.

[1] M. B. Kruger and R. Jeanloz, Science **249**, 647 (1990).
[2] J. S. Tse and D. D. Klug, Science **255**, 1559 (1992).
[3] P. Gillet, J. Badro, B. Varrel, and P. F. McMillan, Phys. Rev. B **51**, 11262 (1995).
[4] J. Badro, J.-L. Barrat, and P. Gillet, Phys. Rev. Lett. **76**, 772 (1996).
[5] J. Pellicer-Porres, A. M. Saitta, A. Polian, J. P. Itie, and M. Hanfland, Nat. Mater. **6**, 698 (2007).
[6] J. S. Tse, D. D. Klug, J. A. Ripmeester, S. Desgreniers, and K. Lagarec, Nature **369**, 724 (1994).
[7] S. L. Chaplot and S. K. Sikka, Phys. Rev. B **47**, 5710 (1993).
[8] B. Kalkan, T. G. Edwards, S. Raoux, and S. Sen, J. Chem. Phys. **139**, 084507 (2013).
[9] K. K. Pandey, N. Garg, K. V. Shanavas, S. M. Sharma, and S. K. Sikka, J. Appl. Phys. **109**, 113511 (2011).
[10] M. Xu, Y. Meng, Y. Q. Cheng, H. W. Sheng, X. D. Han, and E. Ma, J. Appl. Phys. **108**, 083519 (2010).
[11] S. V. Demishev, Y. V. Kosichkin, A. G. Lyapin, N. E. Sluchanko, M. M. Aleksandrova, V. I. Larchev, S. V. Popova, and G. G. Skrotskaya, J. Non-Cryst. Sol. **97**, 1459 (1987).
[12] V. V. Brazhkin, A. G. Lyapin, S. V. Popova, and N. V. Kalyaeva, J. Mat. Sci. **30**, 443 (1995).
[13] V. V. Brazhkin, A. G. Lyapin, S. V. Popova, and R. N. Voloshin, Phys. Rev. B **51**, 7549 (1995).
[14] V. V. Brazhkin, A. G. Lyapin, L. G. Khvostantsev, V. A. Sidorov, O. B. Tsiok, S. C. Bayliss, A. V. Sapelkin, and S. M. Clark, Phys. Rev. B **54**, 1808 (1996).
[15] A. V. Sapelkin, S. C. Bayliss, A. G. Lyapin, V. V. Brazhkin, J. P. Iitié, A. Polian, S. M. Clark, and A. J. Dent, Phys. Status Solidi B **198**, 503 (1996).
[16] A. V. Sapelkin, S. C. Bayliss, A. G. Lyapin, V. V. Brazhkin, M. Clark, A. J. Dent, J. P. Itie, and A. Polian, Mater. Sci. Forum **228–231**, 543 (1996).
[17] S. K. Lee, P. J. Eng, H.-k. Mao, Y. Meng, M. Newville, M. Y. Hu, and J. Shu, Nat. Mater. **4**, 851 (2005).
[18] P. F. McMillan, M. Wilson, D. Daisenberger, and D. Machon, Nat. Mater. **4**, 680 (2005).
[19] A. P. Hammersley, S. O. Svensson, M. Hanfland, A. N. Fitch, and D. Hausermann, High Press. Res. **14**, 235 (1996).
[20] G. Kresse and J. Furthmüller, Comp. Mater. Sci. **6**, 15 (1996).
[21] P. E. Blöchl, Phys. Rev. B **50**, 17953 (1994).
[22] G. Kresse and D. Joubert, Phys. Rev. B **59**, 1758 (1999).
[23] M. P. Allen and D. J. Tildesley, *Computer Simulation of Liquids* (Oxford University Press, New York, 1989).
[24] J. P. De Neufville, S. C. Moss, and S. R. Ovshinsky, J. Non-Cryst. Sol. **13**, 191 (1974).
[25] S. R. Elliott, Nature **354**, 445 (1991).
[26] S. R. Elliott, J. Non-Cryst. Sol. **182**, 40 (1995).
[27] C. Massobrio and A. Pasquarello, J. Chem. Phys. **114**, 7976 (2001).
[28] M. Fábián, E. Sváb, V. Pamukchieva, A. Szekeres, S. Vogel, and U. Ruett, J. Phys. Conf. Ser. **253**, 012053 (2010).
[29] M. Bauchy, M. Micoulaut, M. Boero, and C. Massobrio, Phys. Rev. Lett. **110**, 165501 (2013).

[30] V. V. Struzhkin, A. F. Goncharov, R. Caracas, H. K. Mao, and R. J. Hemley, Phys. Rev. B **77**, 165133 (2008).

[31] N. Mateleshko, V. Mitsa, M. Veres, and M. Koos, J. Optoelectron. Adv. Mater. **7**, 991 (2005).

[32] See Supplemental Material at http://link.aps.org/supplemental/10.1103/PhysRevB.94.195211 for extra results and discussion.

[33] M. Vaccari, G. Garbarino, S. N. Yannopoulos, K. S. Andrikopoulos, and S. Pascarelli, J. Chem. Phys. **131**, 224502 (2009).

[34] L. Properzi, M. Santoro, M. Minicucci, F. Iesari, M. Ciambezi, L. Nataf, Y. LeGodec, T. Irifune, F. Baudelet, and A. DiCicco, Phys. Rev. B **93**, 214205 (2016).

[35] S. Minomura, *Solid State Physics under Pressure* (Terra Scientific, Tokyo, 1985).